This is a repository copy of *Acoustic Method for Determination of the Thermal Properties of Nanofluids*.

White Rose Research Online URL for this paper:
http://eprints.whiterose.ac.uk/152607/

Version: Accepted Version

An acoustic method for determination of the thermal properties of nanofluids

Bashar Mahmoud [a]*, Hugh P. Rice [a], Lee Mortimer [a], Michael Fairweather [a], Jeffrey Peakall [b], David Harbottle [a]

[a] School of Chemical and Process Engineering, and [b] School of Earth and Environment, University of Leeds, Leeds LS2 9JT, UK

*bgy9bm@leeds.ac.uk

ABSTRACT

This study determines the thermophysical properties of nanofluids using ultrasonic techniques. Using an acoustic test cell, fitted with 4 MHz high-temperature transducers, measurements of the speed of sound in an aqueous dispersion of alumina nanoparticles (Al_2O_3, 99.9%, spherical, d_p = 50 nm) are made at volume fractions from 1-5 vol% over the temperature range 20-90°C. The observed relationships between the measured parameters and speed of sound variation are presented. Available theoretical approaches are reviewed and applied to the data of the study. The speed of sound data together with measurements of density and predictions of thermal conductivity, derived from Lagrangian particle tracking (LPT) simulations, are used to determine

the ratio of specific heats of nanofluids using a modified version of the Bridgman equation. The results demonstrate the effectiveness of the measurement technique, with outcomes elucidating the dependence of the speed of sound on temperature and particle concentration, and hence the influence of these parameters on the thermophysical properties of nanofluids. Using the speed of sound approach and LPT simulations, the predicted thermal values, which have an estimated accuracy of 5-10%, show good agreement with theoretical and experimental results available in the literature for similar operating conditions. This research forms the basis for the use of novel acoustic techniques for online, in situ measurement of nanofluids and their potential applications in solar thermal power systems.

INTRODUCTION

A nanofluid is defined as a dispersion of nanoparticles, typically in the size range 1-100 nm, in a base fluid. Nanofluids were first suggested by Choi in 1995[1] to improve the heat transfer properties of conductive fluids by doping them with small concentrations (1.0 to 5.0 vol%) of nanoparticles. Nanofluid research has since received increased attention, with extensive experimental, theoretical and computational studies being completed[2]. The enhancement in heat transfer characteristics obtained using different types of nanoparticles such as metal oxides, non-metallic and carbon nanotubes is described in the literature[3-8], with substantial thermal properties improvements found[9-13]. The thermal conductivity k of nanofluids, for example, is usually found to be much greater than that predicted by classical models, such as the theoretical work of Maxwell[1]. The most significant enhancement in samples containing Al_2O_3 in water with volume fractions ranging between 1 and 5% is an increase in k of between 2 and 27.5%[5-6]. Conversely, the specific heat of nanofluids was reported to decrease gradually by 0.65% as the nanoparticle concentration increases from 0% to 5%[14].

Wang and Mujumdar[5] stated that there are no general mechanisms that explain the thermophysical enhancements of nanofluids, although possible reasons from a modelling perspective have been proposed, such as: collision of the base fluid molecules with each other; thermal diffusion of nanoparticles within the fluid; collisions between nanoparticles[15]; Brownian motion-induced nano-convection of nanoparticles[16] (as a secondary dynamic mechanism); and high particle specific surface area which presents a large heat transfer surface between the particles and the fluid phase. Additionally, there are several other possible macro-scale explanations such as particle-driven natural convection, convection induced by electrophoresis, and thermophoresis[5]. Further details of each of these mechanisms, and models of them, are given by Lee and Jang[17]. This is in addition to the influence of the liquid-solid interface and interactions at the molecular level; the ordered layering of liquid molecules near the solid particles (e.g. liquid nano-layering)[18, 19]. It is also possible that the improvement of the thermal conductivity of nanofluids occurs at an atomic-scale, since it can be related to the transport of electrons in a medium having negligible electrical resistivity caused by scattering (known as ballistic phonon transport), or surface charge state[5].

Recently, the number of industrial applications that can potentially use nanofluid technology, ranging from renewable energy, nuclear reactors, transportation, electronics as well as biomedicine and food, have received much attention, with the main focus being on increased energy efficiency. In these industries, nanofluids offer the following advantages as compared with conventional heat transfer fluids: heat transfer intensification leading to reduced fluid volumes compared to single-phase fluids; reduced particle clogging as compared with conventional slurries, thus allowing system miniaturization; and adjustable parameters, including flowability, heat capacity[20] and thermal conductivity, by varying the particle type and concentration[21]. On the other hand, nanofluids may have disadvantages such as: increases in pumping power requirements due to

greater pressure drop as a result of increased density relative to the base fluid; long-term particle settling[22] and potential clogging of flow passages; possible damage to pipeline transportation systems by erosion; the high cost of nanoparticle suspensions; and increased axial rises in wall temperature due to degraded specific heat[23].

At present, little is known about the behaviour of nanofluids[5] in a process plant, particularly those with potential use in high-temperature applications (e.g. solar thermal plants). Measurements of nanofluid properties are usually limited by either the ability of available instrumentation or material compatibility of the sensing element. This is unfortunate as such measurements can provide critical information about optimal operating conditions, which is required if nanofluid technology is to be scaled-up for practical use. The use of acoustic techniques has therefore been proposed since they are ideal for characterizing single- and multiphase elastic fluids[24] due to the dependence of the speed of sound on a number of parameters such as density, compressibility and temperature. Furthermore, acoustic measurements provide a multitude of data such as time-of-flight, acoustic impedance and attenuation, and variations in acoustic velocity which can be used to monitor particle settling[25, 26], determine the particle concentration of a dispersion[27], and measure the critical transport velocity of a particle suspension in a flow[28].

The focus of this study is on the use of an ultrasonic technique for the analysis and characterization of water-based nanosuspensions using the sound speed dependence on temperature and concentration[29]. This technique is promising for the characterization of multi-phase systems because it is flexible, cost effective, non-destructive, non-invasive and can operate in dense and optically opaque nanosuspensions[30] with fewer restrictions than optical methods. The current study also demonstrates the potential of acoustic methods to determine the thermophysical properties of nanofluids. This is achieved by first measuring the speed of sound in nanofluids, and then using

this data, together with measurements of density and predictions of thermal conductivity derived from Lagrangian particle tracking (LPT) simulations, to determine the ratio of heat capacities of nanofluids using a modified version of the Bridgman equation. This in situ, online method has potential applications in energy storage where thermofluids such as water and molten salts dosed with nanoparticles are under investigation as thermal transfer fluids and storage media, with their application requiring that they be effectively measured and monitored.

THEORY

A. Speed of sound of nanofluids

The variation of the sound speed in water is anomalous[24] in that it does not vary monotonically with temperature[31]. However, the ultrasound speed in water has been widely investigated as it is easy to obtain, and at the same time water is a fundamental component of many products and reactions used in the chemical industry. Water is therefore widely used as a reference material for the calibration of many acoustic instruments, in manufacturing and laboratory applications[32].

The most likely explanation of these anomalous characteristics is the nature of the structure of liquid water molecules, which are linked together by weak hydrogen bonds to give a complex long range structure[31]. Of particular importance in this connection is the relationship between the compressibility and density of water molecules versus temperature (at standard atmospheric pressure), as given by Kell[33], see Figure 1. As a result, both the compressibility and density of water are relatively high at low temperatures (0-10°C). However, as the temperature of water increases, the compressibility decreases sharply, while density shows an inverse exponential decline over the temperature range 10-100°C. Considering these effects in terms of the sound speed

5

formula as given by the Urick[34] (Eq. (1) below), it is clear that an increase in the temperature of water brings an attendant increase in the sound speed.
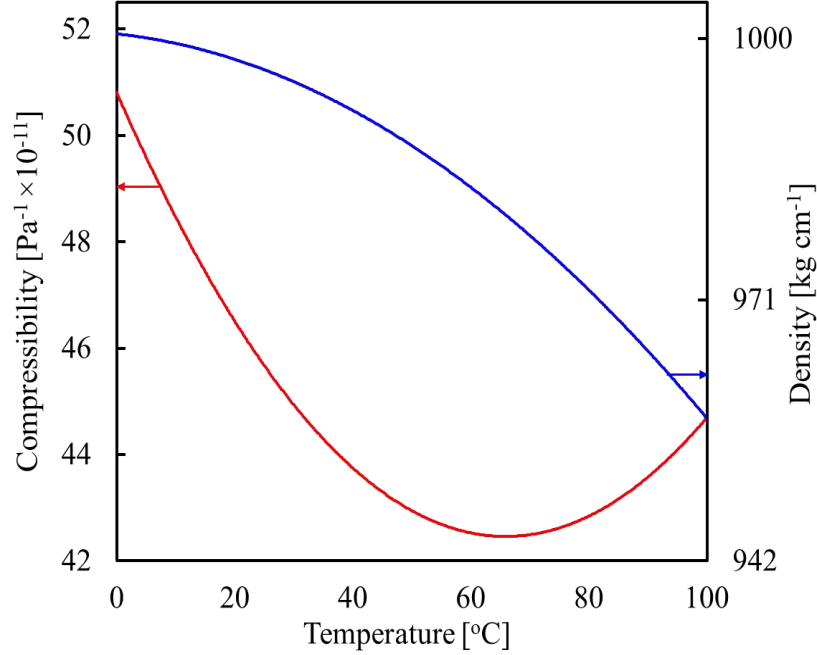

Figure 1. Compressibility and density of water with temperature at standard atmospheric pressure.

Liquid mixtures and homogenous particle dispersions in water are treated by assuming that the speed of sound is mainly affected by the mean compressibility and mean density of the components in the system. This fundamental observation, according to Povey[24], was first made in 1941 by Wood[35], who applied it to liquid mixtures. However, the relationship between the sound velocity in a particle-liquid dispersion can be attributed to Urick[34], hereafter referred to as the Urick equation:

$$ C = \frac{1}{\sqrt{\kappa_s \rho}} \, , \qquad \kappa_s = \sum_j \phi_j \kappa_{sj} \, , \qquad \rho = \sum_j \phi_j \, \rho_j, \qquad (1) $$

where C is the velocity of a sound wave (ms^{-1}) in the dispersion, κ_S the adiabatic compressibility, ρ the density, ϕ the volume fraction of the dispersed phase and the subscript j refers to the

constituent phases. As stated by Povey[24], for one material dispersed within another, the compressibility and density can be written as:

$$\kappa_s = \phi \kappa_{s_2} + (1 - \phi)\kappa_{s_1}, \qquad \rho = \phi \rho_2 + (1 - \phi)\rho_1, \tag{2}$$

where the subscripts 1 and 2 refer to the continuous and dispersed phases, respectively. Eq. (1) and (2) can be used to determine C if κ_s and ρ of both phases are known.

Another form of the Urick equation is[36]:

$$C = \sqrt{\frac{C_p(\gamma - 1)}{\alpha_p^2 T}}, \tag{3}$$

where C_p is the specific heat at constant pressure (isobaric), α_p the coefficient of thermal expansion (at constant pressure), T the absolute temperature, and γ the ratio of heat capacities (also known as the isentropic index), defined as $\gamma = C_p/C_v$, with C_v being the specific heat at constant volume (isochoric). For water at atmospheric pressure C_p, α_p and γ vary considerably with temperature, the net result being an increase in the sound velocity with temperature.

Sound waves propagate as a series of compressions and expansions that change the local kinetic energy of the medium that they pass through. As temperature is a measure of the internal energy of the system, it varies during sound wave propagation. However, the variations in density of the liquid medium take place rather more rapidly with temperature. As a result, the process of heat flow through the test cell (described below) is assumed to be adiabatic. On this basis, Eqs. (1) to (3) are used throughout this study to calculate the sound velocity in both pure water and water-

based nanofluids, assuming the propagation of sound to be adiabatic[24]. For an adiabatic process involving a liquid, both the pressure and volume remain constant.

In principle, measured values of the speed of sound and density of the medium can be used to calculate other thermodynamic parameters that are useful for the modelling of nanofluids. The variation of these parameters with temperature can be calculated from a set of thermodynamic relations using the equation of state (see Supporting Information -A).

B. Predictive correlation between speed of sound and thermophysical properties

The thermal conductivity of a liquid depends on the very rapid transmission of energy via molecular interaction[37]. This mechanism is best understood by considering the speed of sound in liquids, which is five to ten times larger than the speed of motion of the molecules themselves as determined by kinetic theory. The best way to understand the speed of sound in liquids is by considering two colliding molecules, where the energy is transferred instantaneously from the centre of one molecule to the centre of another[37].

Most semi-empirical and theoretical methods used to determine the thermal conductivity, k, of liquids (and suspensions) are based on the empirical relation of Bridgman[38], which assumes that liquid molecules are arranged in a cubic lattice of a particular dimension, and that energy is transferred from one lattice plane to the next at the speed of sound for the given fluid[39]. According to Lin and Pate[40], the theoretical equation of Bridgman[38] was later justified by Powel et al.[41] for the thermal conductivity of liquids. The resulting equation, which can be used for pure fluids, is as follows:

$$k = 2.8 K_B v^{2/3} C,$$

(4)

where K_B is the Boltzmann constant and v the molecular volume of the liquid, that is, the molecular mass divided by the density.

The second formulation is due to Eyring[37], who supposes that only the rotational and translational degrees of freedom are effective in transferring the energy in a polyatomic liquid (e.g. water). Accordingly, the empirical relation of Bridgman[38] can be expressed as:

$$k = 2.8 K_B v^{2/3} \gamma^{-1/2} C. \tag{5}$$

Here, the heat capacity ratio γ (also referred to as the Eucken correction[37]), should be taken as the predicted value from both model simulation and speed of sound measurements. In other words, it is used to convert the isothermal compressibility κ_T to the adiabatic compressibility κ_s measured in speed of sound experiments[37, 42], since sound compression waves are adiabatic in reality, rather than isothermal. According to Hirschfelder[37], Eq. (5) applies extremely well with a mean deviation of around 10% for a large number of liquids. Bridgman also pointed out that his formula gives the correct temperature dependence of the thermal conductivity of liquids at atmospheric pressure[37].

Although most published data on γ are for gases, the importance of γ for liquids is highlighted in a number of studies[37, 43, 44], and it has been referred to as a fundamental physical property of fluids with great importance in reversible adiabatic processes. The value of γ typically varies from 1.30 to 1.66 in gases[42] and from 1.1 to 1.36 in liquids[45], as a function of temperature and pressure. On account of its contribution to sound absorption in liquids, it has been suggested that γ in liquids might be referred to as the sonic anisotropy[43] (the phenomenon that determines the direction of ultrasonic wave propagation and its asymmetry).

As to the theoretical framework and the use of the Bridgman equation[38] (i.e. Eq. (5)), Chebbi[46] developed a model to correlate the speed of sound and thermal conductivity in nanofluids. The results suggest that the enhancement of thermal energy and heat transfer were at the speed of sound in nanofluids (e.g. via consecutive collisions between nanoparticles).

From this it follows that the speed of sound using the Urick equation, Eqs. (1) and (3), can be related to $\gamma, \kappa_S, \kappa_T$ and density as follows:

$$C = \frac{1}{\sqrt{\kappa_s \rho}} = \left(\frac{C_p}{C_v} \frac{1}{\kappa_T \rho}\right)^{1/2} \tag{6}$$

Eq. (4) can now be re-written in terms of the thermodynamic properties as:

$$k = 2.8 K_B v^{2/3} \frac{1}{\sqrt{\kappa_s \rho}} \tag{7}$$

Eq. (5) can be treated similarly:

$$k = 2.8 K_B v^{2/3} \left(\frac{\gamma}{\kappa_T \rho}\right)^{1/2}. \tag{8}$$

Measuring the heat capacity at constant volume C_v can be extremely difficult for liquids and solids because small temperature changes typically produce large pressure changes, meaning that the containing vessel must be able to withstand very high pressure variations. Instead it was decided here to predict the thermal conductivity k for nanofluids at different concentrations and constant pressure using a numerical simulation[47] together with experimental measurements of density and the speed of sound, C, over a range of temperatures. The modified Bridgman equation, Eq. (8), is then used to solve for the heat capacity ratio γ at constant volume, by fitting to equations of the form $\gamma = \gamma(\Phi, T)$ and $k = k(\Phi, T)$.

MATERIALS AND METHODS

A. Materials

Alumina nanoparticles (Al$_2$O$_3$, 80% α/ 20% γ, 99.9% purity) were purchased as a powder from US Research Nanomaterials Inc. Scanning electron microscopy (SEM) of the powder (Figure 2) confirmed particle clusters composed of the primary particles. The supplier reported average particle size was $d_p = 50$ nm and this was experimentally verified using the Zetasizer Nano ZS90 (Malvern Panalytical Ltd.), see Figure 3.
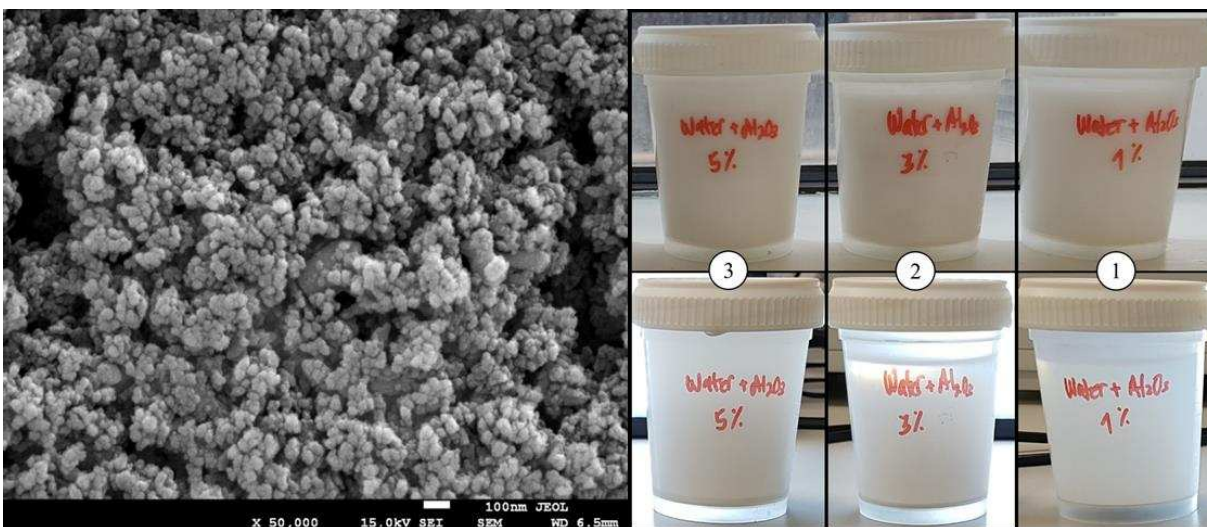

Figure 2. (Left) SEM image of Al$_2$O$_3$ nanoparticles (99.9% pure, $d_p = 50$ nm). (Right) Images of Al$_2$O$_3$ water-based nanofluids, from right to left: 1 water with 1 vol% nanoparticles; 2 with 3 vol%; and 3 with 5 vol%. Samples on the top have been sonicated, samples at the bottom after settling for 4 weeks in the laboratory.

The nanofluids were prepared in distilled water at pH 6.8 and sonicated (505 Sonic Dismembrator, Fisher Scientific) for 250 min to disperse the primary particles. Without sonication the particle size distribution was found to be very broad (Figure 3) with particle clusters greater than a few microns. To enhance particle dispersion and suspension stability, the suspension pH was set at pH = 8.5-9.2 and the particle zeta potential = 24 mV, as measured using the Zetasizer Nano ZS90. Under these

conditions it was possible to disperse the particles to ~50 nm by sonication and the resulting particle suspension was visually assessed to remain stable during the acoustic measurements. Figure 2 (right) shows the results of sonicated specimens versus those at the bottom to settle for four weeks in the laboratory (Figure 2, samples 1, 2 and 3). Although the level of brightness is different between the two sets of images, the photographs clearly show the settled bed of nanoparticles after settling for four weeks.
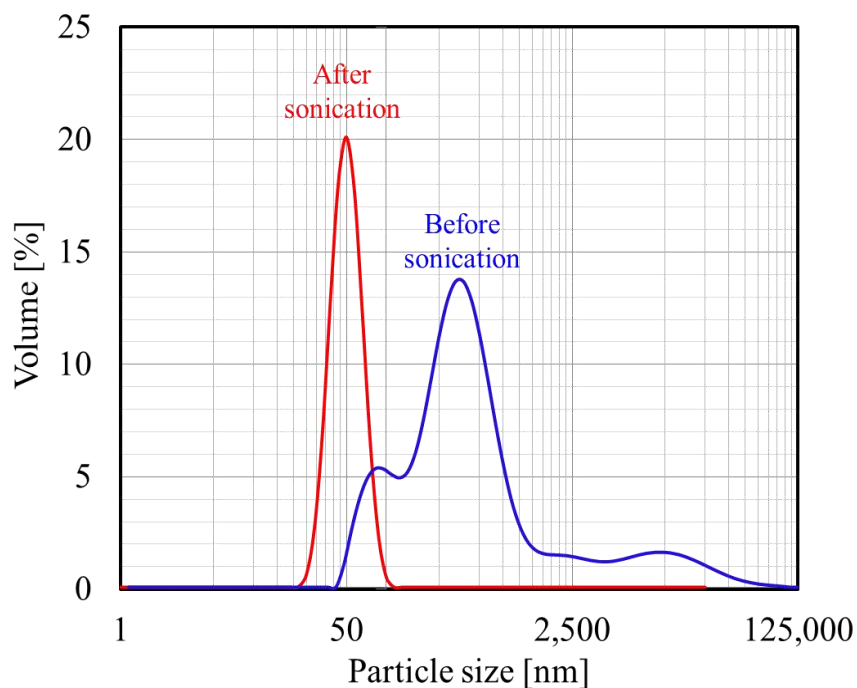

Figure 3. Particle size distribution of Al_2O_3 nanoparticles measured using the Zetasizer Nano ZS90 without (blue) and with (red) sonication.

B. Physical properties of the materials

A detailed description of the physical properties of pure water and the particle species is given with sources in Table 1 and 2, respectively.

Table 1. Physical properties of pure water used as the base fluid.

Parameter	At T=25°C
Sound speed[a], C / ms^{-1}	1493
Thermal conductivity[b], k / W m^{-1}K^{-1}	0.608
Heat capacity[b], C$_p$ / kJ kg^{-1}K^{-1}	4.1796
Density[b], ρ / kg m^{-3}	997.1
Compressibility[c], κ_S / Pa^{-1}	44.8×10^{-11}

The above parameters can be expressed as function of temperature T (in K) as follows:

$$C = 1.40238744\times10^3 + 5.03836171T - 5.81172916\times10^{-2}\,T^2 + 3.34638117\times10^{-4}\,T^3 - 1.48259672\times10^{-6}\,T^4 + 3.16585020\times10^{-9}\,T^5 \quad (C\ \text{in ms}^{-1}, 273\text{ - }373\ \text{K}) \qquad (9)^a$$

$$k_L = -0.2758 + 4.6120\times10^{-3}T - 5.5391\times10^{-6}T^2 \ (k\ \text{in W m}^{-1}\text{K}^{-1}, T_{min} = 273\ \text{K}\ (k_L = 0.57)\ \text{and}\ T_{max} = 633\ \text{K}\ (k_L = 0.424)) \qquad (10)^b$$

$$C_p = 92.053 + -3.9953\times10^{-2}T + (-2.1103\times10^{-4}T^2) + 5.3469\times10^{-7}T^3 \ (C_p\ \text{in J mol}^{-1}\text{K}^{-1}, 273\text{ - }615\ \text{K}) \qquad (11)^b$$

$$\rho_L = 0.14395 / 0.0112^{1+(1-(T/649.727)^{0.05107}}\ (\rho\ \text{in kg m}^{-3}, 273\text{ - }648\ \text{K}) \qquad (12)^b$$

$$\kappa_S = (50.88496 + 0.6163813T + 1.459187\times10^{-3}T^2 + 20.08438\times10^{-6}T^3 - 58.47727\times10^{-9}T^4 + 410.4110\times10^{-12}T^5) / (1 + 19.67348\times10^{-3}T)\ (\kappa_S\ \text{in bar}^{-1}, 273\text{ - }423\ \text{K}) \qquad (13)^c$$

[a] See Ref.[49]

[b] See Ref.[50]

[c] See Ref.[33]

Table 2. Physical properties of the particle species Al$_2$O$_3$ (d$_p$= 50 nm, component purity 99.9%).

Parameter	At T=25°C	Remarks
Sound speed[d], C / ms^{-1}	6420	longitudinal waves
Thermal conductivity[e], k / W m^{-1}K^{-1}	37	
Heat capacity[e], C$_p$ / kJ kg^{-1}K^{-1}	0.775	
Density[d], ρ / kg m^{-3}	3850	
Compressibility[d], κ_S / Pa^{-1}	39.4×10^{-13}	

The above parameters can be expressed as function of temperature T (in K) as follows:

$$k = 5.5 + 34.5 \times \exp.[-0.0033\times(T - 273)]\ (k\ \text{in W m}^{-1}\text{K}^{-1}, 273\text{ - }1573\ \text{K}) \qquad (14)^e$$

$$C_p = 1.0446 + 1.742\times10^{-4}T - 2.796\times10^4T^2\ (C_p\ \text{in kJ kg}^{-1}\text{K}^{-1}, \text{to }1773\ \text{K}) \qquad (15)^e$$

[d] See Ref.[51]

[e] See Ref.[52]

C. Acoustic test cell

A high-temperature test cell was designed to study the thermal performance of nanofluids under both static and dynamic conditions. It consisted of a temperature-controlled cylindrical vessel fitted with an axial agitator (IKA LR 1000, Germany). The cell had a flat base which acted as an acoustic reflector, and the ultrasonic transducers were placed at the top end of the cell facing downwards. The cell was fitted with temperature sensors that allowed measurements to within ±0.01°C. The basic principle of the experimental setup is shown schematically in Figure 4.
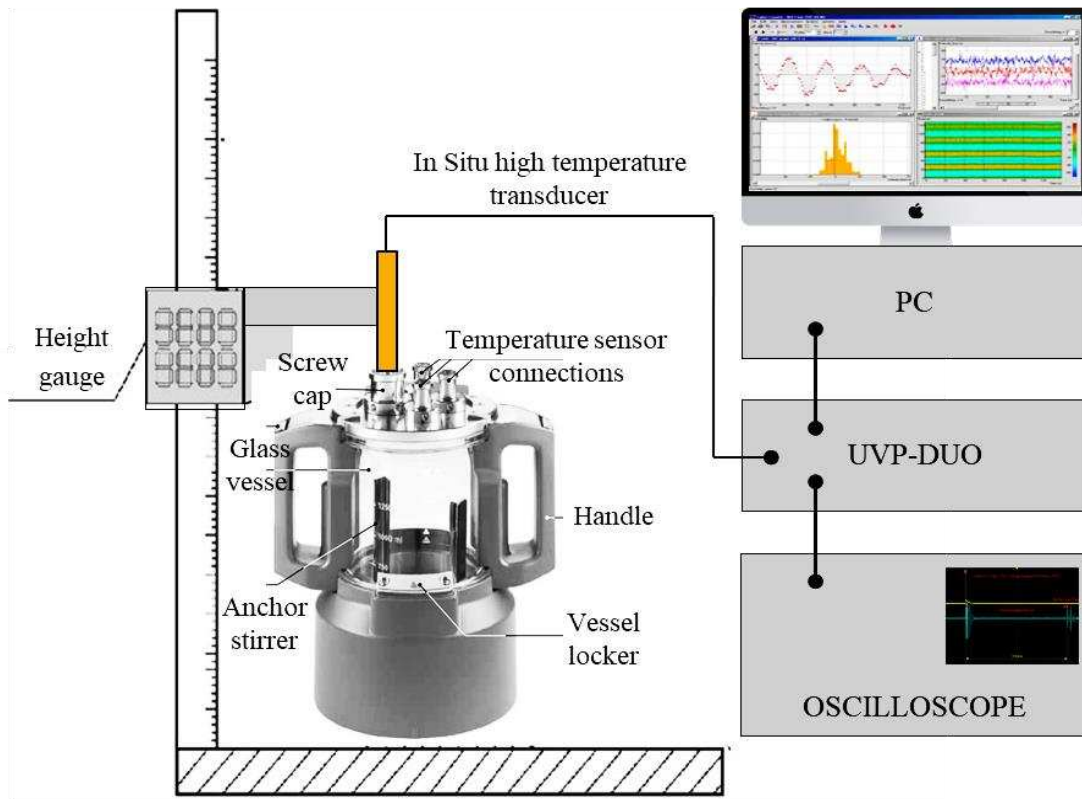

Figure 4. Schematic of the test cell experimental setup for nanofluid sound velocity and thermal conductivity measurements.

An ultrasonic signal processing unit (UVP-DUO, Met-Flow, Lausanne, Switzerland) was used as a signal generator with two ultrasonic emitter-receiver transducers. This ultrasonic systems is

capable of characterizing nanofluids with high precision, with the main sources of uncertainty being the probe position height and the orientation accuracy of the probe giving a combined error of (±0.17mm), the oscilloscope peak-to-peak resolution (±0.18μs) and the uncertainty in temperature measurements (±0.1°C); for further details, see Supporting Information -B. Analysis of these errors demonstrates that the temperature variation is negligible compared to other sources of error (Supporting Information -B).

Two types of emitter-receiver probes were used in this study, both operating at 4 MHz: standard (0-60°C) 4 MHz probes (Imasonic SAS, Besançon, France), active diameter 5 mm; and a high-temperature model (Ionix, Huddersfield, UK) to operate over a wider range of temperatures (–40 °C to +380°C), active diameter 10 mm. A backscattered pressure wave is produced by suspended particles which produces a voltage in the transducer. This echo signal was monitored and displayed on a digital oscilloscope (WaveSurfer 3024, Teledyne LeCroy, Glasgow, UK).

D. Measurements of speed of sound

The test cell was designed such that the transducers were in contact with the nanofluid. The cell operates on a time-of-flight basis over a known distance. The echo voltage signal was recorded by an oscilloscope through the test section of the cell in a vertical, one-dimensional profile. The test section and ultrasonic probe are shown in Figure 5.
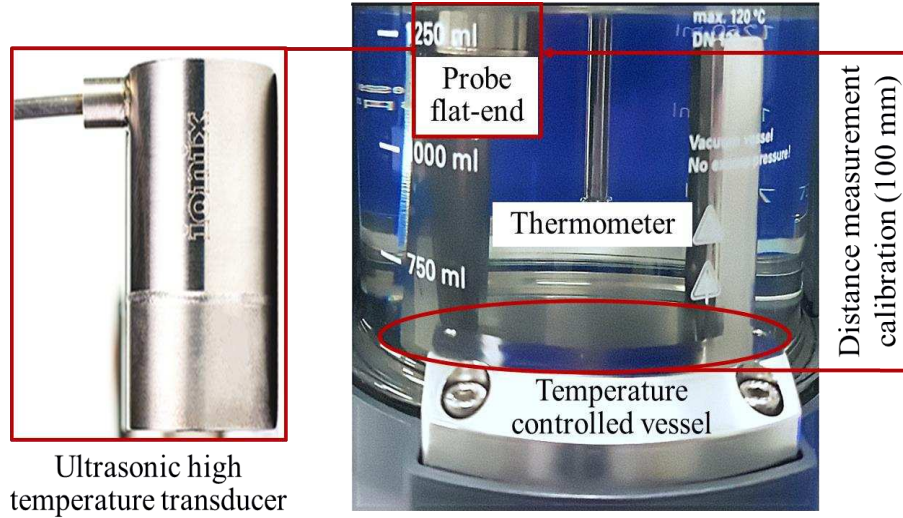
Figure 5. (Left) High-temperature transducer used for the speed of sound measurements. (Right) Photograph of the test section of the nanofluid thermal cell.

A small volume of nanofluid was used (approximately 1 litre) so that the system could be well controlled and all dispersions were degassed and well mixed.

E. Distance calibration

Pure water was used to validate the measurement method because there are reliable, high-precision reference data in the literature. The distance between the probe tips and the base of the cell was set to 100 mm using a height gauge (with accuracy including orientation of probe of ±0.17mm; see Supporting Information -B) as shown in Figure 4, giving a total measurement distance of 200 mm (after travelling through distance h=100 mm, total = 2h). Figure 6 shows the reflected single between the ultrasonic probe and base of the cell.

The ultrasonic signal processing unit was used as a signal generator, and triggered the oscilloscope; see the left side of Figure 6. It was found most appropriate to acquire a waveform within only one triggering interval (the repetition frequency) and repeat the acquisition a number of times for multiple measurements, which were then averaged.
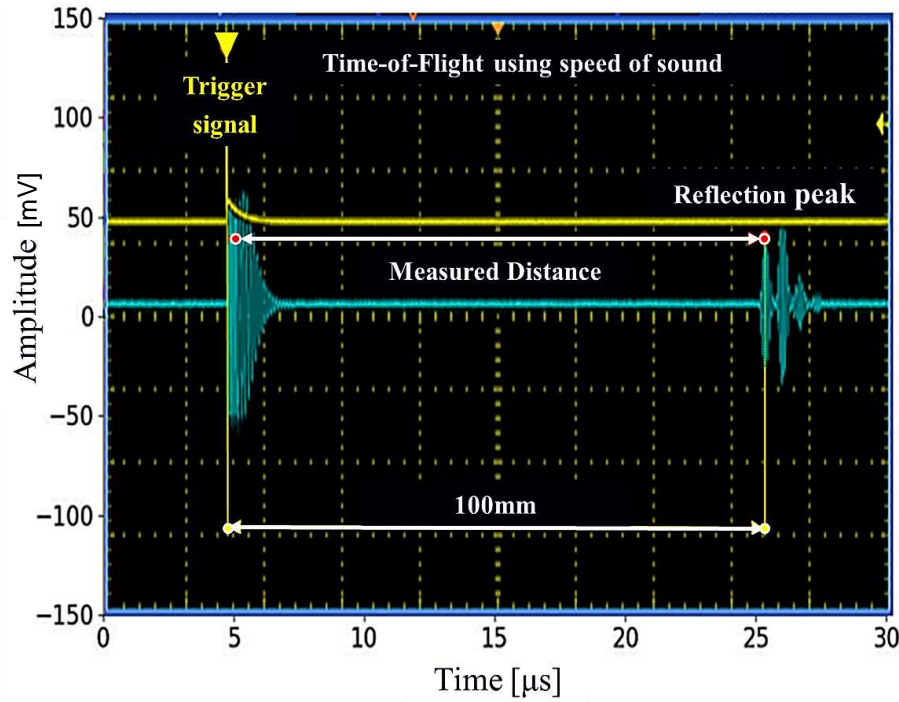
Figure 6. Screenshot of ultrasonic pulse captured by oscilloscope over test distance of 100 mm. Trigger signal in yellow, received signal in blue.

F. Methods of determining nanofluid thermal properties

Quoted values of the thermal conductivity through specific types of material are usually given at a specific temperature. However, no data exist in the literature for the thermal conductivity for this particular type of Al_2O_3 nanoparticle suspension at the required operating conditions, thus it can only be obtained experimentally or by using numerical simulation. Although the conductivity of Al_2O_3-nanofluids could be measured directly via experiments, such measurements are difficult and so the numerical method described here is presented as an alternative approach. Simulation of nanofluids also has the advantage of providing some validation results, as well as enabling a more detailed understanding of the underlying processes, i.e. the dynamics involved in the enhancement of thermal properties via nanoparticle loading.

The simulations were performed using a numerical multiscale model which applies a Lagrangian particle tracking approach[47], capable of detecting the dynamics of, and heat transfer mechanisms in, Al_2O_3 based nanofluids and which is used herein to compute the thermal properties (i.e. thermal conductivity) at various operating conditions (temperatures and concentrations). The three-dimensional computational region examined consisted of a 1μm cube filled with stagnant water. This volume element was composed of a collection of $d_p = 50$ nm Al_2O_3 spherical nanoparticles (40-2000 in number) that were injected uniformly across the domain. Other nanoparticle sizes (25 nm and 71 nm) were also considered within the same volume element.

The motion of the embedded nanoparticles in the fluid is treated using an Eulerian-Lagrangian hybrid scheme with fixed time stepping. Two directions (x and z) used periodic boundary conditions while the third y direction limits were treated as walls. The particle equations of motion were integrated using a fourth order Runge-Kutta scheme with a very small time step, $\Delta t = 10^{-11}$ s. The dynamic properties of both phases were coupled to the ambient temperature of the fluid suspension, that being water at 5 to 95 °C. Further details can be found elsewhere[47].

Using this LPT routine, the force on each particle, at each timestep, was calculated accounting for the particle contact force, electric double layer repulsive force, the van der Waals attractive force, the fluid force and the random Brownian motion force, as shown in the two-dimensional schematic given in Figure 7.
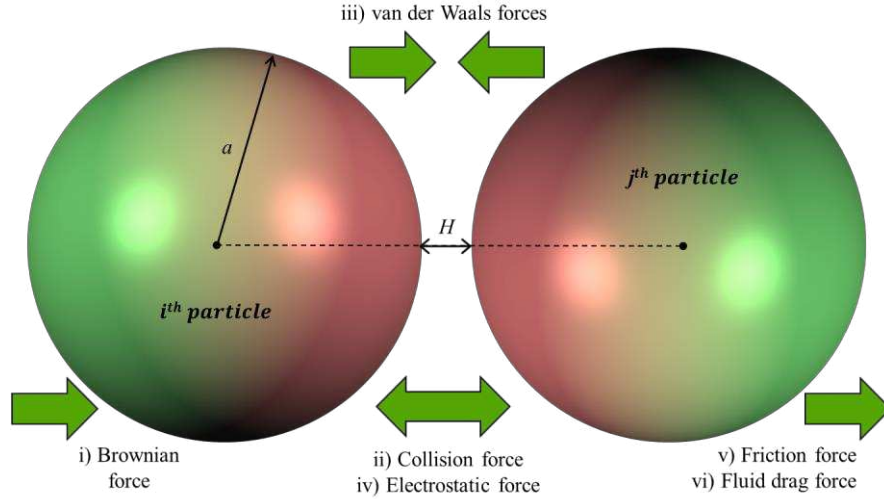
Figure 7. Schematic diagram of the forces acting on two spherical nanoparticles submerged in a fluid continuum: (i) Brownian force; (ii) contact force; the instantaneous balance of the (iii) van der Waals and (iv) electrostatic forces; and the resulting (v) friction and (vi) fluid drag forces.

The model allows the magnitude of the different forces exerted on nanoparticles in a suspension to be predicted, given a set of nanofluid properties. Figure 8 shows the various multiscale forces plotted as a function of the inter-surface distance, H, normalized by the particle radius, a, at 25°C and 90°C. These predictions indicate the magnitude of the various forces exerted on the particles which drive particle collision and aggregation in the computational cell represented in the insert of Figure 8.

These results illustrate that when sufficient distance is maintained between nanoparticles, the effects of both the fluid (drag) and Brownian random motion forces dominate over other contributions since these forces are dependent on the velocity of the nanoparticles and interactions between the particles and the fluid. As the inter-surface distance between particles diminishes, the electric double layer repulsive force starts to have a significant effect on particle interactions. When two particles are close to colliding, the attractive van der Waals forces become dominant

over all others. After a collision of two nanoparticles, the repulsive force increases rapidly and is of a similar magnitude as the attractive force.
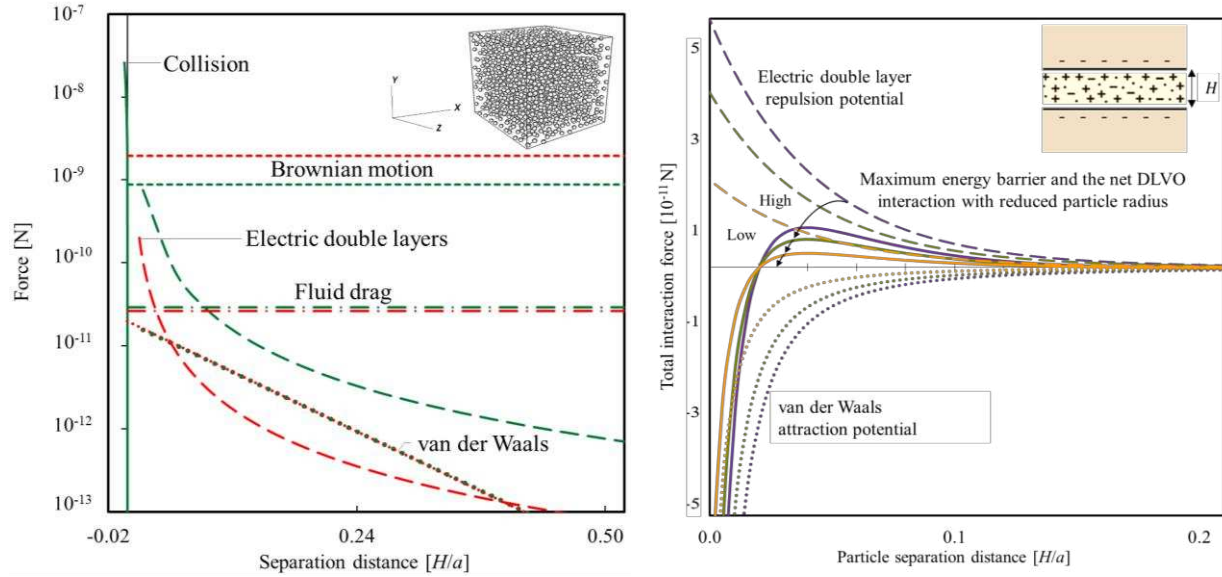

Figure 8. (Left) Magnitude comparison of colloidal and fluid forces as a function of the particle-particle separation distance. The control volume is 1 μm^3 with an Al$_2$O$_3$ content of 1 vol% at 25°C (green) and 90°C (red). (Right) Interaction potential energy versus distance profiles of two colliding Al$_2$O$_3$ nanoparticles at three different sizes: 25 nm (orange); 50 nm (green); and 71 nm (purple). Electric double layer (– –), maximum or total energy barrier (—) and van der Waals (···) forces. The magnitude of the energy is proportional to the particle size (radius) or interaction area (between two planar surfaces).

The nanofluid dynamic model was further coupled to a thermal energy model to predict the overall heat transfer properties of the system which works on the basis of inter-particle distances which are tracked at every time step in the simulation. The technique considers both aggregation kinetics (responsible for the formation of particle percolation pathways) and Brownian motion (responsible for induced micro-convection). These physical phenomena are found to be responsible for the effective thermal conductivity, k$_{eff}$, in nanofluids, and can be expressed mathematically as[47]:

$$k_{eff} = (1 + A\text{Re}^m\text{Pr}^{0.333}\phi)\left\{\frac{[k_{ag} + 2k_{bf} + 2(k_{ag} - k_{bf})\phi_{ag}]}{[k_{ag} + 2k_{bf} - (k_{ag} - k_{bf})\phi_{ag}]}\right\}k_{bf} \qquad (16)$$

where Re is the Brownian Reynolds number, Pr is the Prandtl number, and A and m are constants determined from experiment. Both Re and Pr are calculated from outputs of the numerical model. The dynamic properties of both phases were coupled to the ambient temperature of the fluid suspension, that being water at 25-90 °C. In the above, k_{ag} and k_{bf} represent the thermal conductivity of aggregates and the base-fluid, respectively. The particle volume fraction is given as ϕ for a primary particle and as ϕ_{ag} for aggregated particles that are characterized by their radius of gyration R_a, determined using the mean free path (average distance a particle travels between collisions) and the depth-first search method.

The combined experimental-numerical method presented here has proven to be useful for generating the thermal values of Al$_2$O$_3$-nanofluids at different operating conditions and particle sizes. With the use of the speed of sound measurement that has been determined experimentally, the method enables the ultrasound technique to generate key thermal property date of nanofluids (i.e. the ratio of heat capacities).

RESULTS AND DISCUSSION

A. Measured speed of sound of pure fluid and nanofluids

All sound velocity measurements were made with the acoustic test cell described in the previous section, the results of which are shown in Figure 9. The figure shows the change in acoustic time measured by the oscilloscope in pure water, over the temperature range of 25-85°C. These data were used to find the peak-to-peak resolution needed for the propagation of error analysis, and

were also used for the thermometer sensor calibration over a given temperature range (see Supporting Information -B).

The influence of Al$_2$O$_3$ particle concentration on the speed of sound was measured up to 5 vol%, using both transducers, as illustrated in Figure 10.
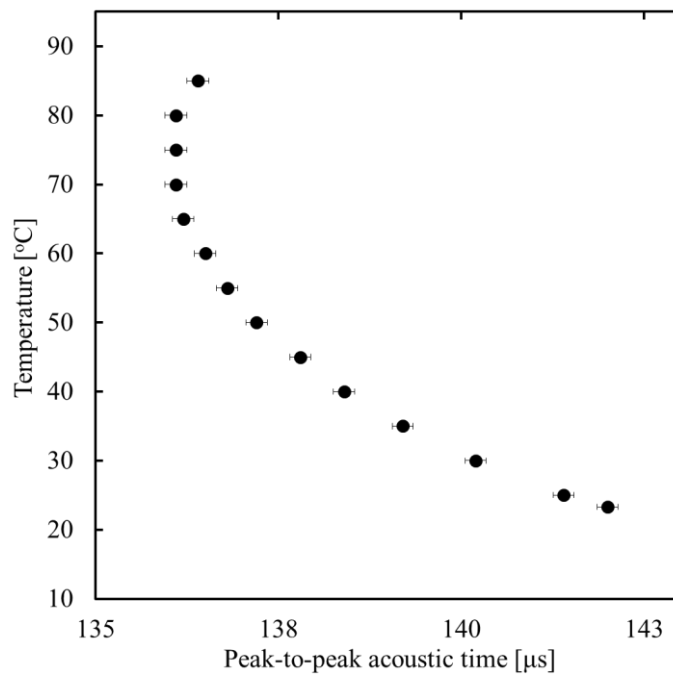

Figure 9. The change in the peak-to-peak time base of ultrasonic signals collected by the oscilloscope with temperature, for pure water.
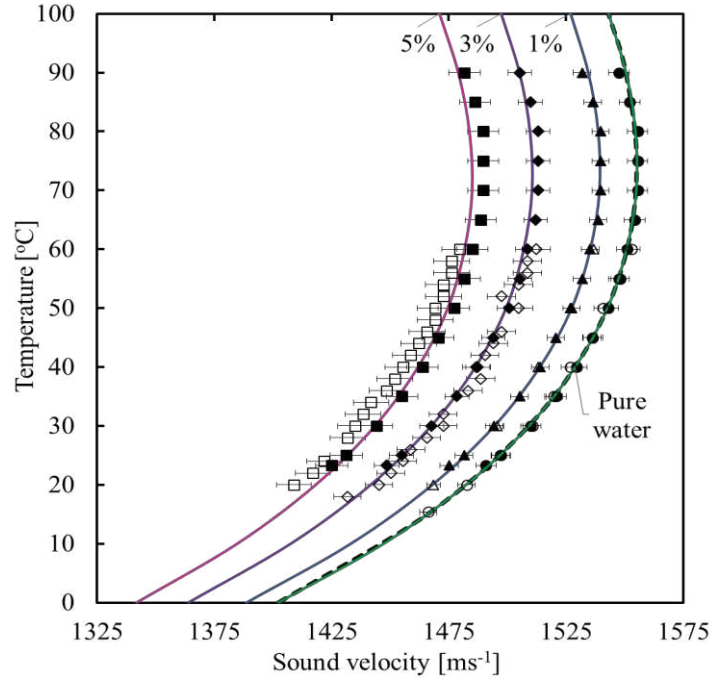
Figure 10. Measured sound velocity in pure water and water-based nanofluids containing $d_p = 50$ nm alumina (Al_2O_3) as a function of temperature and concentration. Open symbols: standard transducer. Closed symbols: high-temperature transducer. Circles: pure water; triangles: 1 vol%; diamonds: 3 vol%; squares: 5 vol%. Colours indicate theoretically calculated values at various solid concentrations using Urick[34] equation. Dashed: experimental data of Bilaniuk and Wong[49].

As shown in Figure 10, the results confirm the accuracy of the sound speed measurements for pure water, when compared to predictions of the Urick[34] equation and the data of Bilaniuk and Wong[49]. The sound velocity increases until it reaches a maximum at about 74°C. Thus, the temperature coefficient dC/dT is positive up to this temperature. The velocity then decreases with increasing temperature >74°C, hence dC/dT is negative from this point onward.

Figure 10 also shows the sound velocity in water-based nanofluids containing $d_p = 50$ nm Al_2O_3 nanoparticles. The sound velocity increases with increasing temperature until, in all cases, it again reaches a maximum at about 74°C, similar to that shown for pure water.

The slight differences between the low and high temperature transducer results can be attributed to their different frequency of operation, since the high temperature transducer has a centre frequency ≈ 3.45 MHz, whereas the standard transducer has a corresponding frequency ≈ 4.0 MHz. The results demonstrate that the velocity of sound is frequency-dependent for this type of nanosuspension system. It should also be noted that very minor influences of distance measurements when using the two probes are likely to impact on the value of the sound velocity in the test mixture. Such errors are indicated by the error-bars, with the variation of ultrasonic velocity with probe distance discussed in detail in Supporting Information -B.

Additionally, the standard probe was found to be more sensitive to the effect of reflection and attenuation of ultrasound waves caused by the presence of high nanoparticle concentrations. This can be seen by the minor discrepancies between the two transducer types at a solids concentration of 3 vol%, and then more noticeably at 5 vol%. Other potential errors could have contributed to differences between the two sets of measurements, although the small volumes of nanofluid tested, especially with the high-temperature transducer, were continuously calibrated, very well mixed, and fully dispersed. Accordingly, the Urick[34] equation is in closest agreement with the more reliable high temperature transducer data.
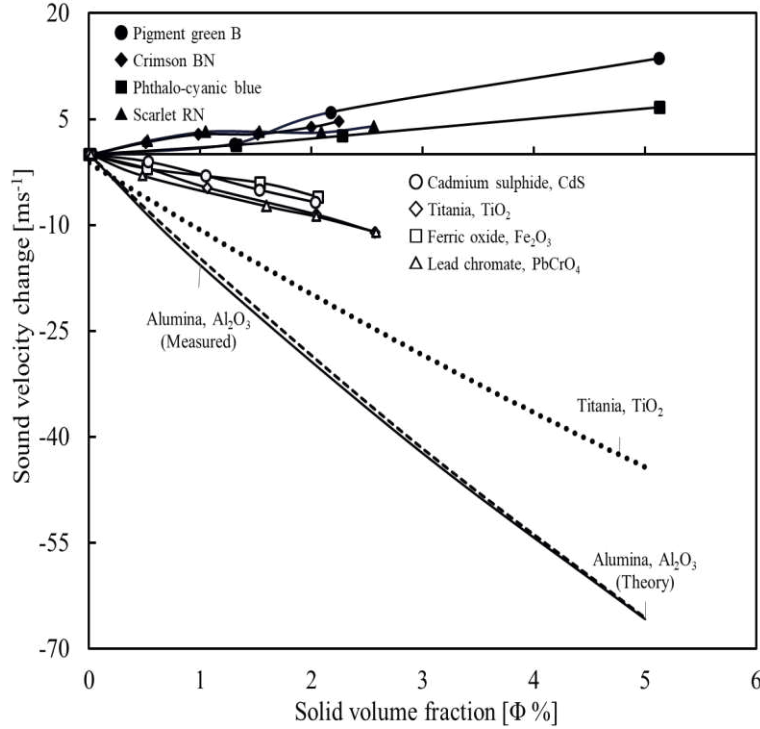
Figure 11. Relation of ultrasound velocity change through dispersions of light and heavy solid particles in water or Turkish oil. Solid: sound velocity in alumina (Al_2O_3) nanofluid. Dashed: theoretically calculated values using Urick[34] equation. Data of Piotrowska[53] (Closed symbols: light solids. Open symbols: heavy solids). Dotted: experimental data of Kim et al.[29].

The main observation from these results is the decrease in sound velocity with increasing particle concentration. To describe this phenomenon, the change in sound velocity measurements at room temperature is plotted against the concentration of $d_p = 50$ nm alumina particles, together with the results obtained by Piotrowska[53] and Kim et al.[29], in Figure 11.

It should be noted that in the data of Piotrowska[53] a mixture of distilled water with Turkish oil (stabilizer) was used as the dispersive phase for the particle species, with the exception of TiO_2, and scarlet RN, where distilled water was used alone. The study[53] reported that it was possible to obtain accurate results at low concentrations up to 2% using an interferometric method, whereas the method used here can go up to 5% and is only limited by attenuation and the thermal interaction at higher voltages. It is clear that the sound velocity in suspensions of lighter species (e.g. pigment

green B, Crimson BN, see densities Table 3), which are also partly soluble in water, was higher than that of suspensions of heavier species (i.e. TiO_2, Fe_2O_2) that are not soluble either in water or in water with Turkish oil. The physical properties of all particle species used in the figure are shown in Table 3.

Table 3. Physical properties of particle species.

Species	Density, ρ / kg m^{-3}
Alumina, Al_2O_3	3850
Titania, TiO_2*	3840
Ferric oxide, Fe_2O_3*	4740
Lead chromate, $PbCrO_4$*	4540
Cadmium sulfide, CdS*	-
Pigment green B*	1560
Crimson BN*	1460
Phthalo-cyanic blue*	-
Scarlet RN*	1400
Titania, TiO_2**	3980

*Species used by Piotrowska[53] had irregular shapes and undefined particle size in the micrometer range. **Species used by Kim et al.[29] were spherical and had an average size of 55 nm with a secondary peak at around 200 nm.

The data of Kim et al.[29] for water-based TiO_2 nanofluids shown in Figure 11 indicate that in the concentration range 0 to 5 vol% the velocity decreases as the concentration increases. An important implication of this finding in the case of low particle concentrations is the wide interparticle distance, which was thought by Kim et al.[29] to be the cause for the reduction of ultrasound wave propagation (due to scattering). Kim et al.[29] also showed that the sound velocity decreases until nanoparticle concentrations reach $\sim 30\%$, above which the sound velocity increases due to the small interparticle distance and rapid wave propagation through the particles. Further details of this complex multiple scattering phenomena are given by Kim et al.[29]

It can also be observed that the nano-sized TiO_2 used by Kim et al.[29] decreased the speed of sound more than the micro-sized TiO_2 particles used by Piotrowska[53] (i.e. by 30 ms^{-1}), which is an

important observation supporting the effect of particle size on the speed of sound measurements (Figure 11).

B. Implementation of predictive method for thermal conductivity

In this section results of the LPT methodology used to underpin predictions of the thermal conductivity of Al_2O_3-nanofluids are validated in order to provide confidence in the accuracy and ability of the method. The determined thermal conductivity values were validated against experimental measurements and other model predictions from a number of sources[54-59], with good agreement found, as shown in Figure 12. The model is also capable of predicting the effect of concentration and nanoparticle size on the overall thermal conductivity of the system, giving predictions (coloured) which are in good agreement with experimental data (Beck et al.[54]) that examined heat conduction in nanofluids using seven sizes of alumina nanoparticles ranging from 8 to 282 nm in diameter.
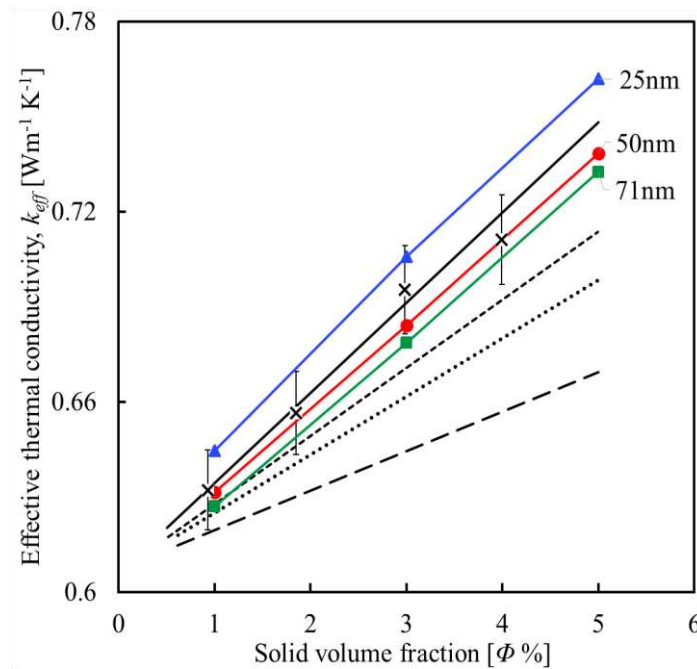
Figure 12. Effective thermal conductivity of nanofluid containing 71nm spherical Al_2O_3 particles as a function of volume fraction Φ. Experimental data of Beck et al.[54] ($\times$), with error bars from that source. Theoretical work of Maxwell[55] is shown for spherical particles ($\cdots$). Lines represent predictions of Nan et al.[57] (– –); Yu and Choi[58] (----); and Warrier et al.[59] (—). Present work: predictions using numerical model[47] at different particle sizes: 71nm (-■-); 50nm (-●-); 25nm (-▲-).

Regarding size dependence, the present model predicts that the conductivity of nanofluids containing $d_p = 25$ nm Al_2O_3 particles is greater than those containing 50 nm and 71 nm particles, by nearly 8% and 15%, respectively, although no systematic experimental investigation of size-dependant conductivities has been performed. Conversely, in Beck et al.[54] it is indicated that the thermal conductivity enhancement decreases as the particle size decreases below about 50 nm and they attributed this decrease in enhancement to a decrease in the thermal conductivity of the nanoparticles themselves (as the particle size becomes small enough to be affected by increased phonon scattering). Their measurements showed a clear effect of the particle size and dispersion method (e.g. mixing/sonication) and indicate that there is an expected limit of enhancement for nanofluids containing larger nanoparticles. Their results were found to be marginally within the predictions of the present study. It should be noted that although the results given in Figure 12 show the effect of volume fraction on the thermal conductivity, the existing model showed more sensitivity to particle size in predictions of conductivity than the model of Beck et al.[54].

The theoretical values of the Maxwell[55] model presented in Figure 12 were found to be slightly below the results of the present model. This classical model of Maxwell[55] is widely used to determine the effective electrical or thermal conductivity of liquid-solid suspensions of monodisperse, low-volume-fraction mixtures of spherical particles. It involves the particle size/shape and volume fraction and assumes diffusive heat transfer in both fluid and solid phases. The model may give good predictions for micron-sized particles, but generally underestimates the

magnitude of thermal conductivity enhancement in nanosuspensions as a function of volume fraction[17].

Figure 12 also shows predictions made using the numerical model of Nan et al.[57] that attempts to account for the effects of: particle size, shape, distribution and volume fraction; the orientation of inclusions; and the interfacial thermal resistance on the conductivity of nanofluids. Their model was developed in terms of an effective medium approach combined with Kapitza's thermal contact resistance concept, suitable for the prediction of thermal conductivity of mineral matrix composites[57].

The predictions of Yu and Choi[58] were derived using a modified version of the Maxwell equation that includes the effect of liquid molecules close to the solid surface of nanoparticles on the thermal conductivity of solid-liquid suspensions. This effect assumes the formation of layered solid-like structures (known as ordered nanolayers) which have a major impact on nanofluid conductivity, in particular when the particle diameter is less than 10 nm. Although their predictions are found to be slightly below the results derived from the present model, they follow the same overall trend, as shown in Figure 12.

Warrier et al.[59] also modelled the thermal conductivity of nanoparticle suspensions and examined the effect of the two phases present in the heterogeneous system. Their model takes into account adjustable parameters such as the temperature dependence of the thermal conductivities of the individual phases, as well as the size dependence of the dispersed phase. Using this modified version of the geometric mean model allowed the effect of a wide range of particle sizes (11 to 302 nm), volume fractions and temperatures to be studied. It can be seen that the Warrier et al.[59] model predictions fall between the Beck et al.[54] error bars. Although the predictions of Warrier et

al.[59] are slightly above those of the present results, they show approximately the same rate of change in conductivity with solid volume fraction.

It can therefore be concluded that the numerical model described is in good agreement with the experimental data of Beck et al.[54], and the numerical model of Warrier et al.[59], with all these showing very similar gradients in conductivity with solids volume fraction. In contrast, the models of Maxwell[57], Nan et al.[57], and Yu and Choi[58] all under-predict the influence of solid volume fraction on effective thermal conductivity by comparison. This is in agreement with previous work that shows that the Maxwell equation, of which Yu and Choi[58] is a variant, under-predicts this relationship. The Nan et al.[57] simulations under-predict to a far greater degree than any of the other models, suggesting that the approach is not well suited to Al_2O_3 nanoparticle suspensions.

In addition, and with the aim of verifying the above predictions, the normalized thermal conductivity, k_{eff}/k_{bf}, is plotted against temperature and volume fraction in Figure 13.
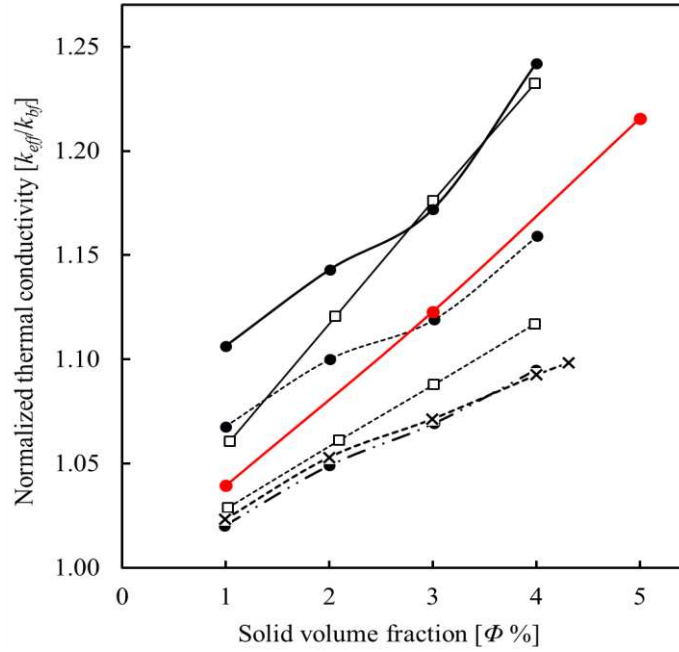
Figure 13. Thermal conductivity of nanofluid containing spherical $d_p = 50$ nm Al_2O_3 particles as a function of volume fraction Φ. Experimental data of Lee et al.[60] at 21°C (--×--). Lines represent the predictions of Das et al.[61] at 25°C (– · · –●), 33°C (--●--) and 51°C (–●–). The theoretical work of Hamilton and Crosser[62] at 21°C is shown for both cylindrical (–□–) and spherical (--□--) models. Present work: predictions using numerical model[47] at 25°C (-●-).

The predicted thermal conductivity values are found to be in good agreement with experimental data and predictions made by the other researchers[60-62] also given in Figure 13, and particularly the data of Lee et al.[600] and Das et al.[61] at the same operating temperature (25°C). This is in addition to agreement with the theoretical model of Hamilton and Crosser[62] for both cylindrical and spherical particles. It is clear from all these results that the thermal conductivity increases roughly linearly as concentration increases from 1 to 4 vol.%.

C. The ratio of heat capacities

The modified Bridgman equation is combined with experimental speed of sound measurements to give a very simple yet accurate semi-empirical model for the prediction of thermal properties. This model is used with predicted thermal conductivity values from simulations to determine the ratio of specific heats (using Eq. (8)) of Al_2O_3-nanofluids at different temperatures and concentrations. Results for the specific heat ratio in the temperate region 25-90°C are shown in Figure 14 alongside the predicted conductivity values.
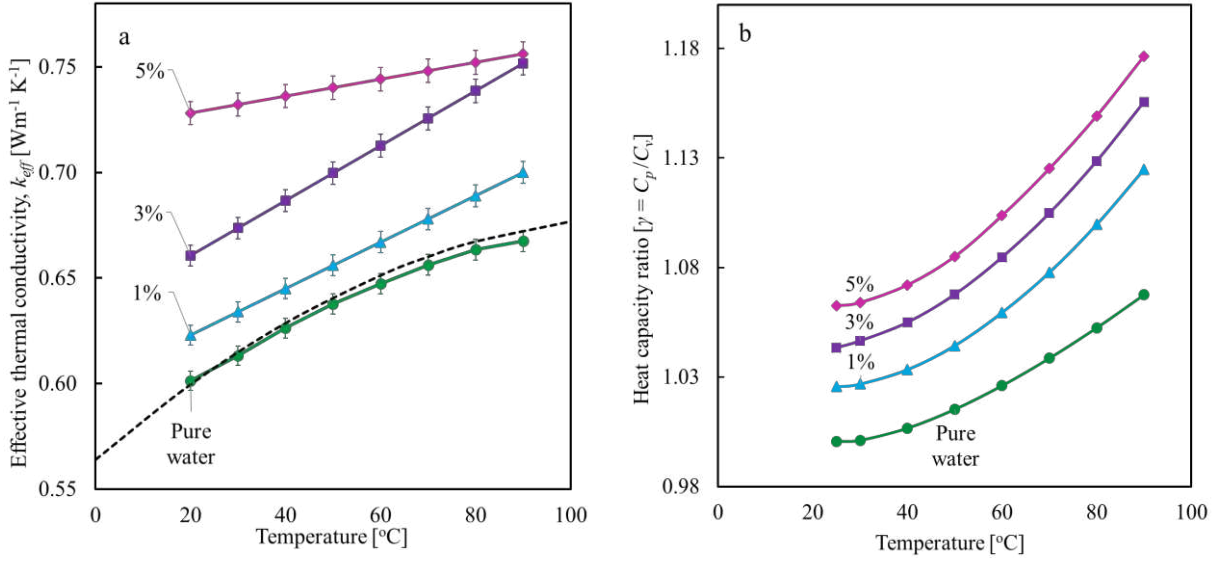
Figure 14. (a) Comparison of thermal conductivity values (— predictions using numerical model[47], ---- experimental data of Coker[63]). (b) Determined heat capacity ratios as function of temperature and concentration of nanofluids (water and spherical d_p = 50 nm Al_2O_3 particles) using Eq. (8).

The predicted thermal conductivity values increase with increasing temperature, supporting the contention that such increases are due to the increased probability of particle collisions and the effects of Brownian motion. The predicted values, at different volume fractions and temperatures, show an almost 12.5% increase for 5 vol.% of particles relative to pure water. Although these predictions were made over a temperature range of 25 to 90 °C, they suggest that further enhancement is to be expected with temperature as a result of increases in kinetic energy and hence in the fluid and Brownian motion forces.

The other interesting observation from Figure 14 is that the variation of thermal conductivity with temperature tends to flatten at concentrations above 3 vol.%, i.e. a change in slope is indicted above such volume fractions, with this behaviour transitioning from pure liquid at low concentrations to linear behaviour beyond 1 vol.%. From the model predictions this demonstrates that the system is entering a different regime where particle collisions driven by Brownian motion

start to increase and as a result induced micro-convection starts to dominate, leading to a substantial increase in thermal conductivity[15]. The increased colloidal forces[20] and aggregation kinetics (collisions; van der Waals forces; electric double layer forces) are also responsible for the formation of nanoparticle percolation pathways, generating more conductive pathways for thermal energy transfer. Similar results were obtained using a combined mechanism-based model of aggregation kinetics with Brownian motion-induced micro-convection.[47]

It can be seen from Figure 14 that the ratio of the heat capacities γ for pure water increases with temperature. Similarly, with the addition of nanoparticles the heat capacity ratio shows an increase with temperature that is most pronounced at 5 vol.%. The reason for this from a modelling perspective is that at higher particle concentrations there are more particles in a system, therefore there is a greater chance that the particles will collide; this in turn increases the collision frequency and thus increases the heat capacity ratio. Moreover, an increase in temperature will raise the average kinetic energy of the particles in the system. Therefore, a greater proportion of particles will have the minimum energy necessary for an effective collision. This ratio can therefore be used in the calculation of the thermal conductivity of Al_2O_3-nanofluids using the modified Bridgman equation, Eq. (8), and vice versa.

These results emphasise the significant effect of temperature and particle concentration on the thermal conductivity and ratio of specific heats. In order to better represent the modification of these thermal parameters with temperature and concentration, the data shown in Figure 14 were used to construct three dimensional plots, plotting both $T-k-\Phi$ and $T-\gamma-\Phi$ surfaces, as illustrated in Figure 15.
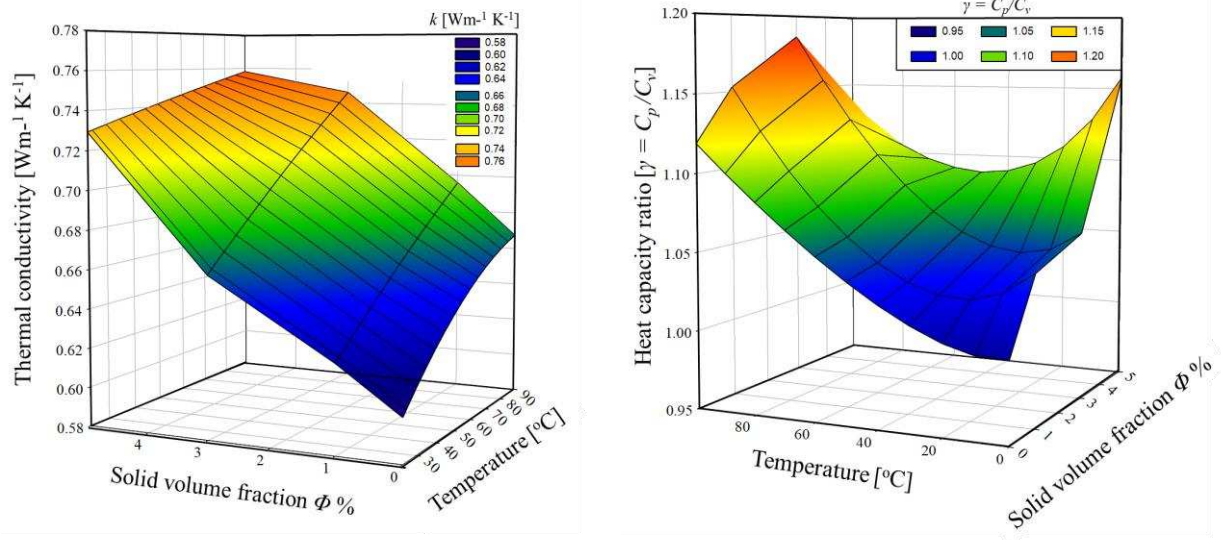
Figure 15. (Left) Dependence of thermal conductivity k on temperature T and solid volume fraction Φ. (Right) Dependence of heat capacity ratio γ on T and Φ, for Al_2O_3 nanofluids.

The effect of particle volume concentrations $\Phi > 3$ vol.% on both k and γ is clear from the results. The enhancement of thermal properties in nanofluids at higher concentrations can be explained by the increased interaction of nanoparticles, as explained above. As to the temperature dependence of the system, which was found to be strong, previous results[47] demonstrated that the enhancements were due to Brownian motion (induced micro-convection) and collisions between nanoparticles as well as aggregation kinetics (the formation of particle percolation pathways) in the base fluid. The increase in temperature leads to an increase in kinetic energy that intensifies both the Brownian motion and particle collisions of Al_2O_3-nanofluids.

These new results confirm the temperature and concentration dependence of both k and γ and the influence of Brownian motion, interparticle collisions and particle size. They confirm that heat transfer enhancement through the use of nanoparticles is a valuable approach for a wide variety of industrial applications, with the use of Al_2O_3-nanofluids in heat exchange devices showing

significant promise and offering increased efficiency and significant energy savings, compared to conventional heat transfer fluids.

Lastly, it may be noted that the ratio of heat capacities derived from the combined LPT simulations and experimental values for the speed of sound used in this study may also be used together with P-V-T relations as a method to obtain values of C_p or C_v for nanofluids using Eq. (S18) and Eq. (S19), as described in Supporting Information -A.

CONCLUSIONS

The limited availability of methods for measuring the thermophysical properties of nanofluids online calls for the development of reliable techniques. The results of a combined experimental and numerical investigation aimed at determining the properties of water-based Al_2O_3-nanofluids using high-temperature ultrasonic transducers, based on the time-of-flight principle, and an Lagrangian particle tracking model were presented. The results show that this combined technique can be used as a simple and reliable method of measuring the speed of sound in nanofluids up to a solid loadings of 5 vol%. The variation of the speed of sound with nanoparticle concentration and temperature was found to be large compared to that in pure water. It was also shown that use of a thermal conductivity model of nanofluids (using a modified version of the Bridgman equation) with measured speed of sound values and the heat capacity ratio gives accurate predictions.

In addition, new data has been generated that is in line with past work on Al_2O_3 nanofluids. These data demonstrate that the addition of nanoparticles to the base liquid enhances the thermal conductivity, with that enhancement increasing with increasing particle concentration and decreasing particle size. This trend is explained by numerical considerations of two mechanisms responsible for thermal conductivity and heat capacity ratio enhancement: Brownian motion

(responsible for induced micro-convection) and aggregation kinetics (responsible for the formation of particle percolation pathways). Future work will extend the advances made in the current study to include a broader selection of thermofluids such as molten nitrate salts under a wide range of operating conditions, especially temperature, to cover those found in solar thermal heat storage systems. More specifically, we are currently extending the model described to include the role of oscillatory structural forces, i.e. non-DLVO forces between ceramic nanoparticles, to study their influence on the thermal conductivity of molten salt-based nanofluids.

AUTHOR INFORMATION

Corresponding Authors

*E-mail: *bgy9bm@leeds.ac.uk

ORCID*

Bashar Mahmoud: 0044-7762-086868

Author Contributions

B.M. conceived the study. M.F., J.P, D.H and H.R. supervised the study. B.M. and H.R worked on the theoretical and experimental technique development. B.M. and L.M performed the numerical predictions. All authors analyzed the data, discussed their implications, wrote the paper and revised the manuscript at all stages.
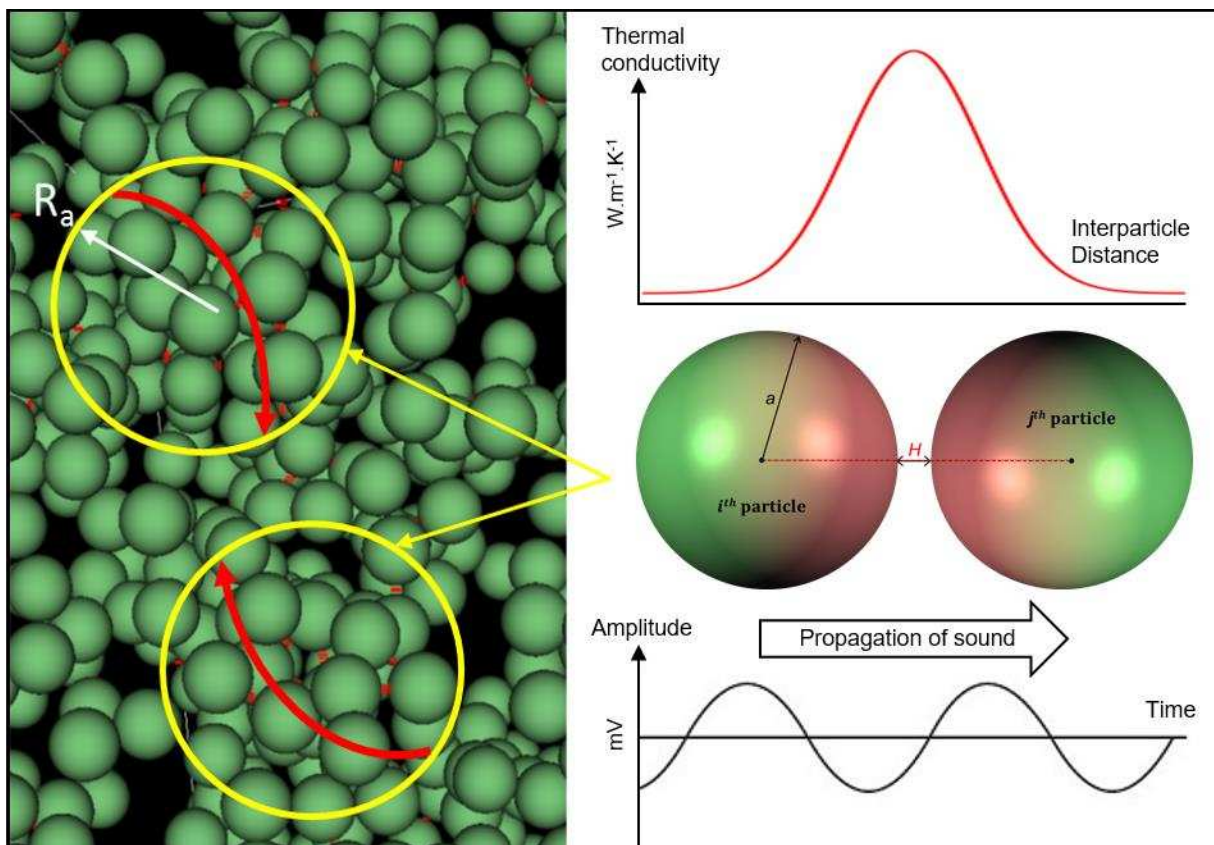
SUPPORTING INFORMATION

A. The derivation of thermodynamic relations between the ratio of heat capacities and the experimental values of the speed of sound. B. The propagation of experimental errors and uncertainty.

REFERENCES

1. Choi, S.U.S. Nanofluids: From vision to reality through research. J. Heat Transf. **2009**, 131, 033106/1– 033106/9.
2. Xuan, Y.; Li, Q. Heat transfer enhancement of nanofluids. Int. J. Heat Fluid Flow **2000**, 21, 58– 64.
3. Wang X.Q.; Mujumdar A.S. Heat transfer characteristics of nanofluids: A review. Int. J. Therm. Sci. **2007**, 46, 1– 19.
4. Shin, D.; Banerjee, D. Effects of silica nanoparticles on enhancing the specific heat capacity of carbonate salt eutectic (work in progress). IJASE **2010**, 2, 25– 31.
5. Wang, X.Q.; Mujumdar, A.S. A Review on nanofluids – Part I: Theoretical and numerical investigations. Braz. J. Chem. Eng. **2008a**, 25, 613– 630.
6. Wang, X.Q.; Mujumdar, A.S. A review on nanofluids – Part II: Experiments and applications. Braz. J. Chem. Eng. **2008b**, 25, 631– 648.
7. Bhanushali, S.; Jason, N.N.; Ghosh, P.; Ganesh, A.; Simon, G.P.; Cheng, W. Enhanced thermal conductivity of copper nanofluids: The effect of filler geometry. ACS Appl. Mater. Interfaces **2017**, 9, 18925− 18935.
8. Azizi, M.; Hosseini, M.; Zafarnak, S.; Shanbedi, M.; Amiri, A. Experimental analysis of thermal performance in a two-phase closed thermosiphon using graphene/water nanofluid. Ind. Eng. Chem. Res. **2013**, 52, 10015– 10021.
9. Shima, P. D.; Philip, J. Role of thermal conductivity of dispersed nanoparticles on heat transfer properties of nanofluid. Ind. Eng. Chem. Res. **2014**, 53 (2) 980– 988.
10. Murshed S.M.S.; Leong K.C.; Yang C. Thermophysical and electrokinetic properties of nanofluids – A critical review. Appl. Therm. Eng. **2008**, 28, 2109– 2125.
11. Yu W.; France D.M.; Routbort J.L.; Choi S.U.S. Review and comparison of nanofluid thermal conductivity and heat transfer enhancements. Heat Transf. Eng. **2008**, 5, 432– 460.
12. Chandrasekhar M.; Suresh S. A review on the mechanisms of heat transport in nanofluids. Heat Transf. Eng. **2009**, 30, 1136– 1150.
13. Wen D.; Lin G.; Vafaei S.; Zhang K. Review of nanofluids for heat transfer applications, Particuology **2009**, 7, 141– 150.
14. Cao, J.; Ding, Y.; Ma, C. Aqueous Al2O3 nanofluids: the important factors impacting convective heat transfer. Heat and Mass Transf. **2014**, 50, 1639– 1648.
15. Prasher, R.; Bhattacharya, P.; Phelan, P.E. Thermal conductivity of nanoscale colloidal solutions (Nanofluids). Phys. Rev. Lett. **2005**, 94, 025901/1– 025901/4.
16. Azizian, R.; Doroodchi, E.; Moghtaderi, B. Effect of nanoconvection caused by Brownian motion on the enhancement of thermal conductivity in nanofluids. Ind. Eng. Chem. Res. **2012**, 51, 1782– 1789.
17. Lee, S.-H.; Jang, S.P. Mechanisms and models of thermal conductivity in nanofluids, in Heat Transfer Enhancement with Nanofluids, Bianco, V.; Manca, O.; Nardini, S.; Vafai, K. (Eds.). CRC Press, Boca Raton, Florida, 2015, 78– 98.

18. Israelachvili, J.N. Intermolecular and surface forces, 2nd Edition, Academic Press, London, 1992.

19. Taha-Tijerina, J.J.; Narayanan, T.N.; Tiwary, C.S.; Lozano, K.; Chipara, M.; Ajayan, P.M. Nanodiamond-based thermal fluids. ACS Appl. Mater. Interfaces **2014**, 6, 4778− 4785.

20. Hong, Y.; Ding, S.; Wu, W.; Hu, J.; Voevodin, A.A.; Gschwender, L.; Snyder, E.; Chow, L.; Su, M. Enhancing heat capacity of colloidal suspension using nanoscale encapsulated phase-change materials for heat transfer. ACS Appl. Mater. Interfaces **2010**, 2, 1685– 1691.

21. Das, S.K.; Choi S.U.; Patel H.E. Heat transfer in nanofluids – A review. Heat Transfer Eng. **2007**, 27, 3– 19.

22. Sen, S.; Govindarajan, V.; Pelliccione, C.J.; Wang, J.; Miller, D.J.; Timofeeva, E.V. Surface modification approach to TiO_2 nanofluids with high particle concentration, low viscosity, and electrochemical activity, ACS Appl. Mater. Interfaces **2015**, 7, 20538– 20547.

23. Lee, J.; Mudawar, I. Assessment of the effectiveness of nanofluids for singlephase heat transfer in micro-channels. Inter. J. Heat Mass Transf. **200**7, 50, 452– 463.

24. Povey, M.J.W. Ultrasonic techniques for fluids characterization, Academic Press, San Diego, 1997.

25. Wedlock, D.J.; McConaghy, C.J.; Hawksworth, S. Automation of ultrasound velocity scanning for concentrated dispersions. Colloids and Surfaces A: Phy. Eng. Aspects **1993**, 77, 49– 54.

26. Locatelli, F.; François, P.; Laurent, J.; Lawniczak, F.; Dufresne, M.; Vazquez, J.; Bekkour, K. Detailed velocity and concentration profiles measurement during activated sludge batch settling using an ultrasonic transducer. Sep. Sci. and Tech. **2015**, 7, 1059– 1065.

27. Rice, H.P.; Fairweather, M.; Peakall, J.; Hunter, T.N.; Mahmoud, B.; Biggs, S.R. Measurement of particle concentration in horizontal, multiphase pipe flow using acoustic methods: Limiting concentration and the effect of attenuation. Chem. Eng. Sci. **2015**, 126 , 745– 758.

28. Rice H.P.; Fairweather M.; Peakall J.; Hunter T.N.; Mahmoud B.; Biggs S.R. Constraints on the functional form of the critical deposition velocity in solid-liquid pipe flow at low solid volume fractions. Chem. Eng. Sci. **2015**, 126, 759– 770.

29. Kim, J.; Kim, J.; Bae, M.; Ha, K.; Kim, M.; Chu, M. Analysis of the dependence of the sound speed in a nano-particle suspension on the concentration of nano-paticles. New Physics: Sae Mulli **2017**, 67, 243– 247.

30. Rice H.P.; Fairweather M.; Hunter T.N.; Mahmoud B.; Biggs S.; Peakall J. Measuring particle concentration in multiphase pipe flow using acoustic backscatter: Generalization of the dual-frequency inversion method. J. Acoust. Soc. America **2014**, 136, 156– 169.

31. Asher, R.C. Ultrasonic Sensors, Institute of Physics, London, 1997.

32. National Institute of Standards and Technology, Gaithersburg MD, 20899, https://doi.org/10.18434/T4D303, (accessed December 9, 2018).

33. Kell, G.S. Density, thermal expansivity, and compressibility of liquid water from 0° to 150°C: Correlations and tables for atmospheric pressure and saturation reviewed and expressed on 1968 temperature scale. J. of Chem. and Eng. Data **1975**, 20, 97– 105.

34. Urick, R.J. A sound velocity method for determining compressibility of finely divided substances. J. of Appl. Phy. **1947**, 18, 983– 987.

35. Wood, A.B.A. Textbook of sound, Bell and Sons, London, 1941.

36. Blitz, J. Fundamentals of ultrasonics, Butterworth & Co. Ltd., London, 1963.

37. Hirschfelder, J.O.; Curtiss, C.F.; Bird R.B. Molecular theory of gases and liquids, John Wiley and Sons, New York, 1954.

38. Bridgman, P.W. The compressibility of thirty metals as a function of pressure and temperature. Proc. Am. Acad. Arts Sci. USA **1923**, 58, 165– 242.

39. Bird, B.R.; Stewart, W.E.; Lightfoot, E.N. Transport phenomena. John Wiley & Sons, New York, 2007.

40. Lin J.Y.; Pate M.B.; A thermal conductivity prediction method for refrigerant mixtures in the liquid phase. IRACC 175 **1992**.

41. Powell, R.E.; Roseveare, W.E.; Eyring, H. The constants of the Beattie-Bridgeman equation. Ind. Eng. Chem. **1941**, 33, 430– 435.

42. Touloukian, Y.S.; Makita, T. Thermophysical properties of matter, - The TPRC data series, Volume 6, Specific heat - Nonmetallic liquids and gases, Plenum Press, New York, 1970.

43. Parthasarathy, S. The ratio of specific heats as a fundamental physical property of liquids. Annalen der Physik **1956**, 452, 178– 184.

44. Bardakov, R.N.; Kistovich, A.V.; Yu. D. Chashechkin calculation of the sound-propagation velocity in inhomogeneous liquid. Doklady Akademii Nauk **2008**, 420, 324– 327.

45. Richards, N.E.; Brauner E.J.; Bockris, J.O.'M. Determination of the velocity of ultrasonic vibrations in molten salts. B. J. Appl. Phys. **1955**, 6, 387– 390.

46. Chebbi, R. A theoretical model for thermal conductivity of nanofluids. Mater. Express **2017**, 7, 51– 58.

47. Mahmoud, B.H.; Fairweather, M; Mortimer, L.F.; Peakall J.; Rice, H.R.; Harbottle, D. Prediction of stability and thermal conductivity of nanofluids for thermal energy storage applications. Computer-Aided Chem. Eng. **2018**, 43, 61– 66.

48. US Research Nanomaterials Inc., 2018. [online] Available at: www.us-nano.com/inc/sdetail/13136 [Accessed 25 Nov. 2018].

49. Bilaniuk, N.; Wong, G.S.K. Speed of sound in pure water as a function of temperature. J. Acoust. Soc. America 1993, 93, 1609– 1612.

50. Yaws, C.L. Chemical Properties Handbook. McGraw-Hill: New York, 1999.

51. Lide, D.R. Handbook of chemistry and physics, 71st Edition, CRC Press, Boca Raton, 1990.

52. Auerkari, P. Mechanical and physical properties of engineering alumina ceramics. Technical Research Centre of Finland, ESPOO, 1996.

53. Piotrowska, A. Propagation of ultrasonic waves in suspensions and emulsions, 1. Investigation of emulsions and pigment suspensions by an acoustic method. Ultrasonics **1971**, 9, 14– 20.

54. Beck, M.P.; Yuan, Y.; Warrier, P.; Teja, A.S. The effect of particle size on the thermal conductivity of nanofluids. J. Nanopart. Res. **2009**, 11, 1129– 1136.

55. Maxwell, J.C. A treatise on electricity and magnetism, 3rd Edition, Clarendon Press, Oxford, 1892.

56. Kaye, G.W.C. and Laby, T.H.. Tables of physical and chemical constants, Longmans Green and Co. Ltd., London, 1995.

57. Nan, C.W.; Birringer, R.; Clarke, D.R.; Gleiter, H. Effective thermal conductivity of particulate composites with interfacial thermal resistance. J. Appl. Phys. **1997**, 81, 6692– 6699.

58. Yu, W.; Choi, S.U.S. The role of interfacial layers in the enhanced thermal conductivity of nanofluids: A renovated Maxwell model. J. Nanopart. Res. **2003**, 5, 167– 171.

59. Warrier, P.; Yuan, Y.; Beck, M.P.; Teja, A.S. Heat transfer in nanoparticle suspensions: Modeling the thermal conductivity of nanofluids. AIChE J. **2010**, 56, 3243– 3256.

60. Lee, S.; Choi, S.U.S.; Li, S; Eastman, J.A. Measuring thermal conductivity of fluids containing oxide nanoparticles. ASME J. Heat Transf. **1999**, 121, 280– 289.

61. Das, S.K.; Putra, N.; Thiesen, P.; Roetzel, W. Temperature dependence of thermal conductivity enhancement for nanofluids. J. Heat Transf. **2003**, 125, 567– 574.

62. Hamilton, R.L.; Crosser, O.K. Thermal conductivity of heterogeneous two-component systems. I&EC Fundam. **1962**, 1, 182– 191.

63. Coker, A.K. Ludwig's applied process design for chemical and petrochemical plants, Gulf Professional Publishing, Houston, 2007.

For Table of Contents Only